J. Plasma Physics (2004), *vol.* 70, *part* 4, *pp.* 415–429.
DOI: 10.1017/S0022377803002666 Printed in the United Kingdom

Periodic and solitary waves of the cubic–quintic nonlinear Schrödinger equation

LIU HONG[1], ROBERT BEECH[2], FREDERICK OSMAN[2], HE XIAN-TU[3], LOU SEN-YUE[3,4] and HEINRICH HORA[5]

[1]Graduate School, China Academy of Engineering Physics, PO Box 2101, Beijing 100088, People's Republic of China

[2]School of Quantitative Methods and Mathematical Sciences, University of Western Sydney, Locked Bag 1797, Penrith South DC 1797, Australia

[3]Institute of Applied Physics and Computational Mathematics, PO Box 8009, Beijing 100088, People's Republic of China

[4]Department of Physics, Shanghai Jiao Tong University, Shanghai 200030, People's Republic of China

[5]Department of Theoretical Physics, University of New South Wales, Sydney 2052, Australia
f.osman@uws.edu.au

(Received 6 November 2003)

Abstract. This paper presents the possible periodic solutions and the solitons of the cubic–quintic nonlinear Schrödinger equation. Corresponding to five types of different structures of the pseudo-potentials, five types of periodic solutions are given explicitly. Five types of solitons are also obtained explicitly from the limiting procedures of the periodic solutions. This will benefit the study of the generation of fast ions or electrons, which are produced from the soliton breaking when the plasma is irradiated a high-intensity laser pulse.

1. Introduction

Since the nonlinear Schrödinger equation (NLSE) model is one of the most important nonlinear models of modern science, many significant contributions have been made in the development of NLSE soliton theory (Serkin and Hasegawa 2000; Zhonghao et al. 2000; Agüero 2001; Hayata and Koshiba 1995). The NLSE appears in many branches of physics, including plasma physics (Farina and Bulanov 2001), nonlinear optics (Mihalach et al. 2002) and quantum electronics, and also in fluid mechanics, the theory of turbulence and phase transitions, biophysics and star formation. Zahkarov and Shabat (1971, 1972) developed the theory of NLSE solitons for the first time. Since then, many applications and experiments have appeared, such as in Boise–Einstein condensates (BEC) (Ruostekoski and Anglin 2001). The study used here is laser interaction with plasmas. When we considered the large amplitude Langmuir wave affected by strong nonlinearity in the fourth-order beating frequency interactions, a series of analytical soliton forms were given in the laser propagating direction. The problem related to ion and electron acceleration, from the breaking of relativistic plasma waves (Modena et al. 1995) and radiative solitons energy in the form of low-frequency electromagnetic

bursts (Sentoku et al. 1999) will be discussed later. In this paper, we consider the dimensionless form of the cubic–quintic NLSE:

$$i\partial_t E + \partial_{xx} E + |E|^2 E - g|E|^4 E = 0, \tag{1}$$

where $E(x,t)$ is a slowly varying complex amplitude of high-frequency electric fields of plasmas and g is the coupling constant of high-frequency fields with electrons, which depends on the electron temperature and density, etc. The dimensional units are defined as

$$E = \frac{\tilde{E}}{\sqrt{16\pi n_0(T_\mathrm{i}+T_\mathrm{e})}}, t = \omega_\mathrm{pe} t', \quad x = \sqrt{\frac{2}{3}}\frac{x'}{\lambda_\mathrm{D}}. \tag{2}$$

The density is

$$n(x,t) = -2|E|^2(1-\gamma|E|^2), \tag{3}$$

where γ is taken as

$$\gamma = \begin{cases} 3(2T_\mathrm{i}+3T_\mathrm{e})/T_\mathrm{e} & \text{(for the fourth-order field)} \\ 0, & \text{(for the second-order field).} \end{cases} \tag{4}$$

Equation (1) describes the amplitude evolution of the fourth-order field's interaction, under the static approximation. In (4), T_i and T_e are the ion and electron temperatures respectively. The dynamic equation involving quintic fields was derived by He (1982) and the Schrödinger equation was studied numerically by He and Zhou (1993). They deduced that the dynamic behavior of the NLSE with an additional high-order Hamiltonian perturbation displayed a nonlinear interaction between Langmuir waves and electrons in plasma. They showed that the quintic nonlinear term leads to a spatio-temporal complexity of wave fields. Ying and Tan (1996) extended (1) to a (2+1)-dimensional cubic–quintic NLSE with fully periodic boundary conditions in order to study the propagation of laser pulses in plasma. For (1), a special solitary wave solution was obtained (Liu and He 1984) and the recurrence was also discussed numerically (Cloot et al. 1990).

In this paper, we propose to set out a systematic treatment of the possible periodic solutions and the possible soliton structures. In Sec. 2, we change the quintic NLSE to an energy integrable form of a quasi-particle for the envelope wave solutions. In Sec. 3, we study the possible different structures of the pseudo-potentials of the quasi-particle. Five different types of possible structures of the pseudo-potential are plotted. In Sec. 4, using the two possible transformations, we solve the model by means of the ϕ^4 model. In Sec. 5, using the exact known solutions of the ϕ^4 model, we obtain five exact explicit periodic solutions of the quintic NLSE. Under some possible limiting procedures, these periodic solutions tend to five different solitons. In the case of three of these periodic solutions we have included three-dimensional graphics to further illustrate our findings. The last section is a short summary and discussion.

2. Energy integral form of the quasi-particle

In this section, we are looking for the envelope solutions of the quintic NLSE in the form

$$E(x,t) = Q(kx+\omega_1 t)\exp\left[-i\left(\frac{\omega}{2k}x+\omega t\right)\right], \tag{5}$$

https://doi.org/10.1017/S0022377803002666 Published online by Cambridge University Press

where $Q(kx+\omega_1 t)$ is a real function of $kx+\omega_1 t$ and the parameters k, ω, ω_1 are undetermined constants. Letting $\tau = kx+\omega_1 t$ and putting (5) into (4), we obtain an ordinary differential equation for the function $Q(\tau)$,

$$-4gk^2Q(\tau)^5 + 4k^2Q(\tau)^3 - \left(4k^2\omega+\omega_1^2\right)Q(\tau) + 4k^4\frac{\partial}{\partial\tau^2}Q(\tau) = 0. \tag{6}$$

Integrating (6) once with respect to τ, we get

$$-\left(\frac{\partial}{\partial\tau}Q(\tau)\right)^2 + \frac{1}{3}\frac{gQ(\tau)^6}{k^2} - \frac{1}{2}\frac{Q(\tau)^4}{k^2} + \frac{1}{4}\frac{\left(4k^2\omega+\omega_1^2\right)Q(\tau)^2}{k^4} + C = 0, \tag{7}$$

i.e.,

$$\left(\frac{\partial}{\partial\tau}Q(\tau)\right)^2 = \frac{1}{3}\frac{gQ(\tau)^6}{k^2} - \frac{1}{2}\frac{Q(\tau)^4}{k^2} + \frac{1}{4}\frac{\left(4k^2\omega+\omega_1^2\right)Q(\tau)^2}{k^4} + C \tag{8}$$

where C is an arbitrary constant.

In Zhou et al. (1992), the authors have obtained a similar result to (8) ($G \sim Q(\tau)$):

$$\frac{1}{2}\left(\frac{dG}{d\tau}\right)^2 + V(G) = H_0 \tag{9}$$

$$V(G) = -\tfrac{1}{6}gG^6 + \tfrac{1}{4}G^4 - \tfrac{1}{2}\alpha^2G^2. \tag{10}$$

However, in the following studies, H_0 is fixed as zero.

Zhou et al. (1992) also present the pseudoenergy of a classical quasi-particle. Obviously, (9) (or equivalently (8)) is the energy integral of a classical quasi-particle with unit mass. Actually, according to different selections of the constant C (H_0 in (9)) g, k, ω, ω_1, we may easily find many new types of exact periodic solitons.

3. Structures of the pseudo-potential for the quasi-particle

After some detailed analysis, we can find that the pseudo-potential function

$$V(Q(\tau)) = -\frac{1}{6}gQ(\tau)^6 + \frac{1}{4}Q(\tau)^4 - \frac{4k^2\omega+\omega_1^2}{8k^4}Q(\tau)^2 + \frac{C}{2} \tag{11}$$

has five independent characteristic structures for different regions of the parameters g, C, k, ω and ω_1.

In order to give out the possible structures of the pseudo-potential $V(Q(\tau))$ given in (11) for physically positive g, we differentiate (11) once with respect to $Q \equiv Q(\tau)$. The result reads

$$V' = -gQ^5 + Q^3 - \frac{4k^2\omega+\omega_1^2}{4k^4}Q = -gQ\left(Q^2 - \frac{1+\sqrt{\beta}}{2g}\right)\left(Q^2 - \frac{1-\sqrt{\beta}}{2g}\right), \tag{12}$$

with

$$\beta = 1 - 4g\omega - g\frac{\omega_1^2}{k^2}. \tag{13}$$

From (13), we know that when $\beta < 0$, there is no real solution for $V' = 0$, except for $Q = 0$. That means that the pseudo-potential (11) has only one maximum located at $Q = 0$ and there is no minimum. The typical structure for this case is plotted in Fig. 1(a).

https://doi.org/10.1017/S0022377803002666 Published online by Cambridge University Press

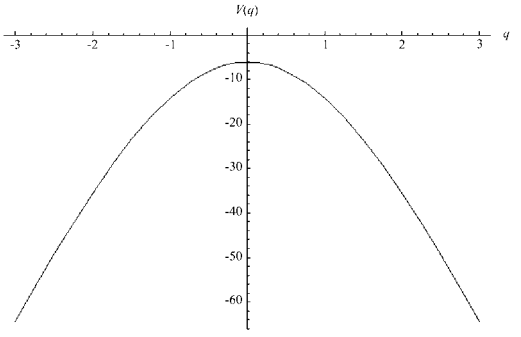

(a)

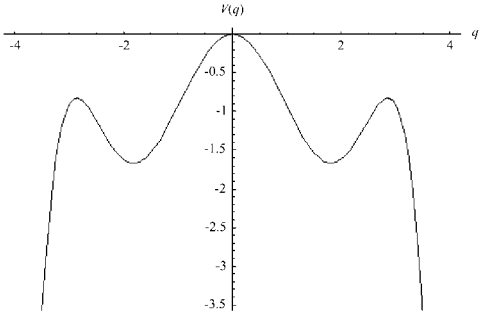

(b)

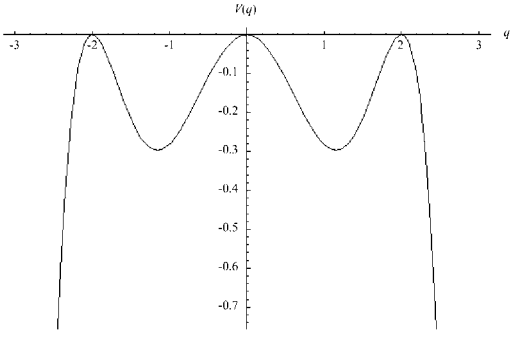

(c)

Figure 1. (a). The plot of (11) for $\beta < 0$. As earlier mentioned, there is no periodic solution in this case. To arrive at this graph we used the parameters of (30) below with $b = 0.055$. This gave a value of $\beta = -0.422\,375$. (b). The parameters used here are the same as for (a) other than that $b = 0.14$, giving $\beta = 0.082\,375$. This is in compliance with the condition set out above. (c) The plot for (11) using the parameters from (37) with $b = 0.3$. (d) The plot for (11) using the parameters from (50) with $a = 1.2575$. (e) The plot for (11) using the parameters from (50) with $a = 0.055$.

If $0 < \beta < 1$, then we have three maxima located at $Q_0 = 0$ and

$$Q_{1\pm} = \pm\frac{1+\sqrt{\beta}}{2g} \tag{14}$$

https://doi.org/10.1017/S0022377803002666 Published online by Cambridge University Press

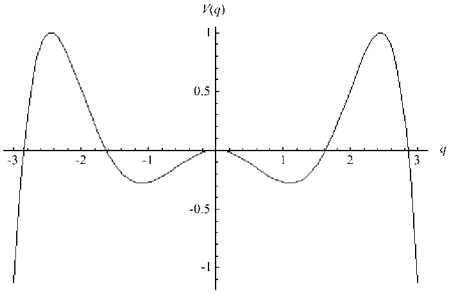

(d)

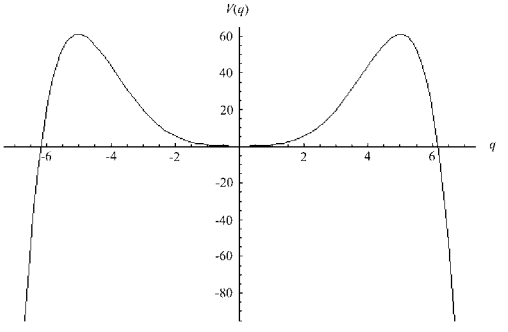

(e)

Figure 1. Continued.

and two minima located at

$$Q_{2\pm} = \pm\frac{1-\sqrt{\beta}}{2g}. \tag{15}$$

In this case, there are three different characteristic structures according to whether the value $V(Q_0)$ is larger than, equal to or less than $V(Q_{1\pm})$. Figure 1(b) is a typical plot of the pseudo-potential for

$$0 < \beta < \tfrac{1}{4}, \quad V(Q_0) > V(Q_{1\pm}). \tag{16}$$

Figure 1(c) is related to the structure of the pseudo-potential with

$$\beta = \tfrac{1}{4}, \quad V(Q_0) = V(Q_{1\pm}) \tag{17}$$

and Fig. 1(d) is a typical structure of the pseudo-potential when

$$\tfrac{1}{4} < \beta < 1, \quad V(Q_0) < V(Q_{1\pm}). \tag{18}$$

The last characteristic structure of the pseudo-potential is related to

$$\beta = 0 \quad \text{or} \quad \beta \geqslant 1. \tag{19}$$

In this case, there exist two maxima located at $Q_{1\pm}$ expressed by (14) and one minimum located at $Q = 0$. Figure 1(e) shows the characteristic structure of the pseudo-potential related to (19).

https://doi.org/10.1017/S0022377803002666 Published online by Cambridge University Press

4. Transformation relations between the ϕ^4 model and the pseudo-energy equation

To find some explicit solutions of the pseudo-energy equation (7) (or (8)), we use the following two transformations

$$Q(\tau) = \frac{\phi_1(\tau)}{\sqrt{a_1\phi_1(\tau)^2 + b_1}}, \tag{20}$$

and

$$Q(\tau) = \frac{1}{\sqrt{a_2\phi_2(\tau)^2 + b_2}} \tag{21}$$

where $\phi_{\rm i}(\tau)$, $i = 1, 2$ are the solutions of the ϕ^4 model

$$(\phi_{{\rm i}\tau}(\tau))^2 = \lambda_{\rm i}\phi_{\rm i}(\tau)^2 + \tfrac{1}{2}\mu_{\rm i}\phi_{\rm i}(\tau)^4 + C_{\rm i}, \quad i = 1, 2. \tag{22}$$

In the transformations (20)–(22), the relations among parameters; $\lambda_{\rm i}, \mu_{\rm i}, C_{\rm i}, g$, C, k, ω and ω_1, read

$$4(3Ca_1 - \lambda_1)k^4 + 4k^2\omega + \omega_1^2 = 0, \quad \big(6Ca_1^2 - \mu_1 b_1\big)k^4 + (4\omega a_1 - 1)k^2 + \omega_1^2 a_1 = 0,$$
$$12Ck^4a_1^3 + \big(-6a_1 + 4g + 12\omega a_1^2\big)k^2 + 3\omega_1^2 a_1^2 = 0, \quad C_1 = b_1 C, \tag{23}$$

and

$$2\big(a_2C_2 - 3Cb_2^2\big)k^4 + (1 - 4\omega b_2)k^2 - \omega_1^2 b_2 = 0, \quad 4(3Cb_2 - \lambda_2)k^4 + 4k^2\omega + \omega_1^2 = 0,$$
$$12Ck^4b_2^3 + \big(12\omega b_2^2 + 4g\big)k^2 + 3\omega_1^2 b_2^2 = 0, \quad 2Ca_2 = \mu_2. \tag{24}$$

Now using the transformation relations (20)–(4) and explicit solutions of the ϕ^4 model, we may obtain many exact solutions of the quintic NLSE.

5. Periodic solutions and solitary wave solutions

Various explicit solutions have been given in terms of the Jacobi elliptic functions (Lou and Ni 1989). In this section we select some of them to write down the exact periodic solutions and the solitons of the pseudo-energy equation (7). It is known that for a quasi-particle, a kink soliton solution is linked with two neighboring degenerated maxima in pseudo-potential. A bell or ring shape linked with a single non-degenerate maximum and the minimum is not the largest point of the pseudo-potential. A periodic solution is related to two non-maximum degenerated points of a potential well. According to these general viewpoints, we know that the kink soliton solutions exist for the cases when the pseudo-potential possesses the structures shown by Figs. 1(c), 1(d) and 1(e); the bell or ring shape soliton solutions are allowed for the structures except for that shown by Fig. 1(a).

From the above discussions, we know that there is no periodic solution and soliton when the pseudo-potential has the characteristic structure of Fig. 1(a).

Selecting $\phi(\tau)$ of (21) as $\mathrm{cn}(\tau)$, we have the first type of periodic solution (5) with

$$Q(\tau) = \pm\frac{1}{\sqrt{a\mathrm{cn}^2(\tau) + b}} \tag{25}$$

https://doi.org/10.1017/S0022377803002666 Published online by Cambridge University Press

while the parameters are related by

$$a = \frac{2g - b - 2k^2b^2(2m^2 - 1)}{4bk^2(m^2 - 1)}, \quad C = \frac{6k^2b^2(2m^2 - 1) - 3b + 2g}{12k^2b^3}, \tag{26}$$

and

$$\omega = -\frac{k^2(2k^2b^2(2m^2 - 1) - 3b + 2g) + \omega_1^2b^2}{12k^2b^3}, \tag{27}$$

with b a root of

$$12k^4b^4 - (8gk^2(2m^2 - 1) + 3)b^2 + 8bg - 4g^2 = 0 \tag{28}$$

and m being the modulus of the elliptic function $\mathrm{cn}(\tau)$. After detailed consideration of the real conditions of b and $Q(\tau)$, we know that the periodic solution (25) with (26)–(28) is related to the periodic motion of the quasi-particle at the potential wells shown in Fig. 1(b). The upper sign of (25) is related to the motion at the right potential well and the lower sign is related to the motion at the left potential well.

Using the definition of the Jacobi elliptical functions (Abramowitz and Stegun 1972), defined as $\mathrm{cn}(\tau)$ is the solution to:

$$\frac{d^2y}{d\tau^2} = -(1 + k^2)y + 2k^2y^3,$$

etc, we know that g is the coefficient of the quintic term in (1) and ω, ω_1 and k are the space–time constants in τ from (5), c is the constant of integration in (11) and m is the modulus of the Jacobi elliptical functions cn, sn and dn. From Abramowitz and Stegun (1972) we know that for $m = 0$, $\mathrm{sn}(\tau) = \mathrm{Sin}(\tau), \mathrm{cn}(\tau) = \mathrm{Cos}(\tau)$ and $\mathrm{dn}(\tau) = 1$. For $m = 1, \mathrm{cn}(\tau) = \mathrm{Sech}(\tau)$, $\mathrm{dn}(\tau) = \mathrm{Sech}(\tau)$ and $\mathrm{sn}(\tau) = \mathrm{Tanh}(\tau)$.

After considering the limiting procedure of (25) for $m \to 1$, we get a symmetric non-topological gray-type soliton.

$$Q(\tau) = \pm\frac{\mathrm{Cosh}(\tau)}{\sqrt{b\,\mathrm{Cosh}^2(\tau) + a}}, \tag{29}$$

with $a > 0,\ b > 0,\ b/2 < g < 3b/4$ $(g > 0)$, and

$$C = \frac{-4g + 3b}{3(-2g + b)b}, \quad \omega = \frac{\omega_1^2b^4 + 4g^2 - 6gb + 2b^2}{2b^2(b - 2g)}, \quad a = \frac{3(2g - b)b}{(3b - 4g)}, \quad k^2 = \frac{2b^2}{2g - b}, \tag{30}$$

for arbitrary b.

We can now show what this looks like in three dimensions by plotting $Q[\tau]$ as a function of space and time. This gives us the very interesting graph shown in Fig. 2.

The simulation presented here for Figs. 1(b), 1(c) and 1(d) are the three-dimensional representation of the soliton equations for each case where a periodic solution occurs and the three-dimensional representation of the envelope equation (5) for the soliton found in each of the above cases. In the case of the soliton equation, the axes represent the amplitude of the soliton, $Q(\tau)$, against space and time. These simulations are produced using the software Mathematica.

Using (29) with these parameters gives the plot shown as (5), for the three-dimensional form of $E[x, t]$, as in the equation. The ring shape soliton (upper line in Fig. 3) is related to the upper sign of (29). The right maximum of Fig. 1(b) and the bell shaped soliton (lower line of Fig. 3) are related to the lower sign of (29) and the left maximum of Fig. 1(b).

https://doi.org/10.1017/S0022377803002666 Published online by Cambridge University Press

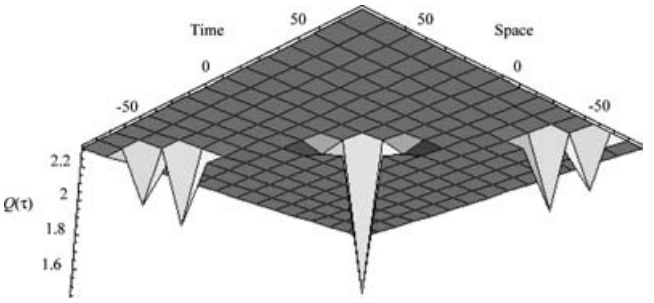

Figure 2. Three-dimensional graph of the soliton produced by (29). This shows the peaks extended downwards, the typical posture of a dark soliton.

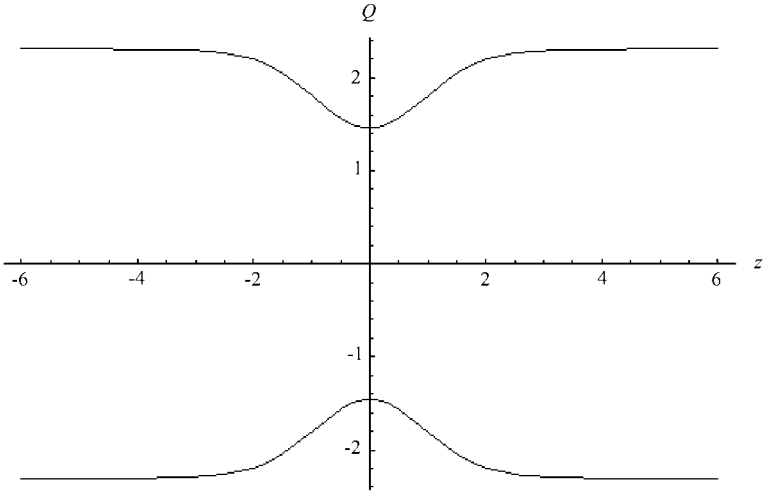

Figure 3. A typical plot of the non-topological dark soliton (29) related to the pseudo-topological structure of Fig. 1(b).

It is known (Lou 2001) that when a further nonlinear effect is included in the model, there may be three effects on the solitons of the model. The first effect is that the old exact solutions are changed by perturbation. In this case, we can use many kinds of perturbation theory to study the new effect on the old exact solutions. The second effect is that the old exact solutions are totally destroyed. This type of case would occur when the old solutions are not stable. The third effect is that some new types of exact solutions may be induced. These types of solutions can be treated by perturbation. From (30), we know that when $g = 0$, k becomes purely imaginary, so this type of soliton can exist only for $g \neq 0$. In other words, the non-topological soliton (5) with (29) and (30) is induced by the quintic term of the NLSE and cannot be treated by perturbation from the cubic NLSE.

The corresponding periodic solution related to the structure of the pseudo-potential shown in Fig. 1(c) reads

$$Q(\tau) = \pm \frac{\mathrm{cn}(\tau)}{\sqrt{a\mathrm{cn}^2(\tau) + b(1 + \mathrm{sn}(\tau))^2}}, \tag{31}$$

https://doi.org/10.1017/S0022377803002666 Published online by Cambridge University Press

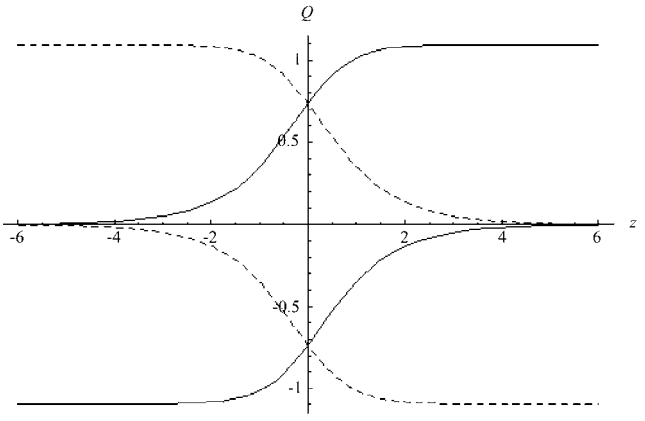

Figure 4. The typical plot of the asymmetric topological kink (solid lines) and anti-kink (dotted lines) soliton (36) related to the pseudo-potential structure of Fig. 1(c).

and can be obtained by taking $\phi(\tau)$ in (20) as

$$\phi(\tau) = \frac{\mathrm{cn}(\tau)}{1 + \mathrm{sn}(\tau)}. \tag{32}$$

In this case, the parameters are related by

$$\omega = -\frac{gm^2}{12a^2} - \frac{8g - 9a}{12a^2} - \frac{12a^2\omega_1^2 - 8ag + 4g^2 + 3a^2}{48a^4k^2} - \frac{4g^2 + 3a^2 + 4a^2k^2g - 8ag}{48a^4k^2m^2}, \tag{33}$$

$$b = -\frac{3a^3k^2(m^2 - 1)}{3a^2k^2(m^2 + 1) - 3a + 2g}, \quad C = \frac{3a^2k^2(m^2 + 1) - 3a + 2g}{12a^3k^2} \tag{34}$$

for arbitrary b.

Figure 4 shows the typical plot of the asymmetric topological kink and anti-kink soliton (36) related to the pseudo-potential structure of Fig. 1(c) for k is determined by

$$8ag - 4g^2 - 3a^2 - 4g(m^2 + 1)a^2k^2 + 12a^4k^4m^2 = 0 \tag{35}$$

with arbitrary a, g, ω_1 and the modulus m of the Jacobi elliptic functions. Solution (31) with the upper sign and (33)–(35) describes the periodic motion of the quasi-particle at the right potential well of Fig. 1(c), while the lower sign describes the motion at the left potential well.

A special type of asymmetric topological kink soliton linked with two right (left) neighboring degenerated maxima of Fig. 1(c) can be obtained from the limiting procedure of (31) with upper (lower) sign $m \to 1$:

$$Q(\tau) = \pm\frac{\mathrm{Exp}[\tau]}{\sqrt{a\mathrm{Exp}[2\tau] + b}} \tag{36}$$

where

$$k^2 = \frac{3}{16g}, \quad \omega = -\frac{64\omega_1^2g^2 - 9}{48g}, \quad a = \frac{4}{3}g, \quad C = 0. \tag{37}$$

The upper two lines of Fig. 4 are the kink and anti-kink related to two right neighboring degenerated maxima of Fig. 1(c) and the lower two lines are the kink

https://doi.org/10.1017/S0022377803002666 Published online by Cambridge University Press

and anti-kink related to the two left neighboring degenerated maxima. From (37), we can see that this type of soliton is also induced by the quintic term of the NLSE and cannot be treated as the perturbation of the cubic NLSE.

For the structure of the pseudo-potential shown by Fig. 1(d), there exist two types of periodic solutions. The first type of periodic solution is related to the motion of quasi-particle at the large potential well between two degenerated maxima while the second type of periodic solution is related to the motion of quasi-particle at the left or right small potential well only. The periodic solution related to the large potential well can be obtained by selecting $\phi(\tau) = \mathrm{sn}(\tau)$ in (20):

$$Q(\tau) = \pm\frac{\mathrm{sn}(\tau)}{\sqrt{a\mathrm{sn}^2(\tau) + b}}, \tag{38}$$

and the relations among the parameters now read

$$\omega = \frac{1}{2}(m^2+1)k^2 + \frac{3}{4a} - \frac{g}{2a^2} - \frac{\omega_1^2}{4k^2}, \tag{39}$$

$$C = -\frac{(m^2+1)}{2a} + \frac{2g-3a}{12a^3k^2}, \quad b = \frac{12k^2a^3}{2g - 6a_2(m^2+1)k^2 - 3a} \tag{40}$$

while a is a root of

$$12(m^2-1)^2k^4a^4 + 8g(m^2+1)k^2a^2 - 3a^2 + 8ga - 4g^2 = 0. \tag{41}$$

When the modulus m of the Jacobi elliptic function $\mathrm{sn}(\tau)$ tends to one, the periodic solution (38) with (39)–(41) becomes a symmetric topological kink for upper sign or anti-kink for lower sign.

$$Q_2(\tau) = \pm\frac{\mathrm{Tanh}(\tau)}{\sqrt{a\mathrm{Tanh}^2(\tau) + b}} \tag{42}$$

with

$$C = -\frac{1}{3}\frac{-2g+3a}{(-2g+a)a}, \quad b = -3a\frac{a-2g}{3a-2g}, \quad k^2 = \frac{(a-2g)(3a-2g)}{16ga^2} \tag{43}$$

and

$$\omega = -\frac{-48g^3a + 32g^2a^2 + 12ga^3 + 64\omega_1^2a^4g^2 + 16g^4 - 9a^4}{16ga^2(a-2g)(3a-2g)}. \tag{44}$$

Figure 5 shows the structure of the symmetric topological kink (continuous curve) and anti-kink (dotted curve). From (43) and (42), we can see that when g tends to zero, k and ω tend to ∞, b tends to $-a$ and then the soliton will be induced by the quintic term of the NLSE and cannot be treated as the perturbation of the cubic NLSE. Figure 6 represents Fig. 5 in three dimensions.

The periodic solution

$$Q(\tau) = \pm\frac{\mathrm{cn}(\tau)}{\sqrt{a\mathrm{cn}^2(\tau) + b}} \tag{45}$$

related to the right (upper sign of (45)) or left (lower sign of (45)) small potential well can be obtained by selecting $\phi(\tau) = \mathrm{cs}(\tau)$ in (20) with the parameter relations

$$b = -\frac{12k^2a^3(m^2-1)}{6k^2a^2(2m^2-1) - 3a + 2g}, \quad C = \frac{6k^2a^2(2m^2-1) - 3a + 2g}{12k^2a^3}, \tag{46}$$

https://doi.org/10.1017/S0022377803002666 Published online by Cambridge University Press

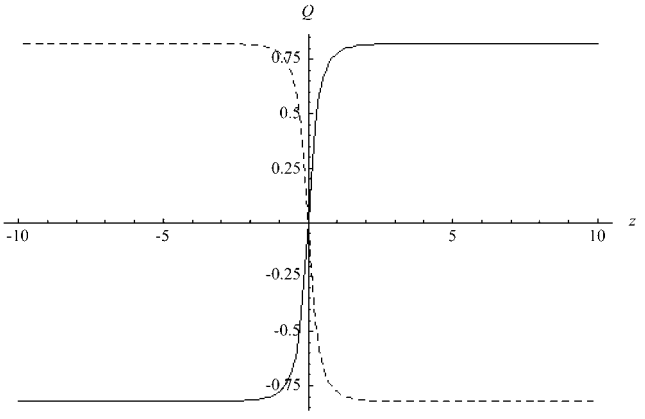

Figure 5. A typical plot of the first type of symmetric topological kink (continuous curve) and anti-kink (dotted curve) soliton (42) related to the pseudo-potential structure of Fig. 1(d).

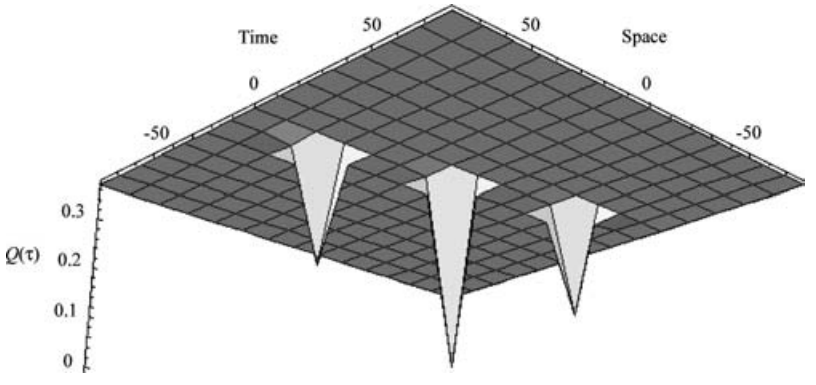

Figure 6. The three-dimensional form of (42), the axes referring to the equation. It goes without saying that we have here another 'dark' soliton. Here we show the view from below, as in Fig. 2.

and

$$\omega = \frac{1}{2}(1-2m^2)k^2 - \frac{\omega_1^2}{4k^2} + \frac{3}{4a} - \frac{g}{2a^2} \tag{47}$$

while a is a solution of

$$12k^4a^4 - 8g(2m^2-1)a^2k^2 - 4g^2 - 3a^2 + 8ag = 0. \tag{48}$$

When $m \to 1$, the periodic solution (45) with (46)–(48) reduces to a symmetric non-topological dark soliton:

$$Q(\tau) = \pm\frac{\mathrm{Sech}(\tau)}{\sqrt{a\mathrm{Sech}^2(\tau) + b}}. \tag{49}$$

In this case, the parameters should satisfy the conditions $0 < g < 9/48k^2$, $C = 0$ and

$$b = -2a + \frac{1}{2k^2}, \quad g + \frac{3}{2}a(2ak^2 - 1) = 0, \quad \omega = k^2 - \frac{\omega_1^2}{4k^2}. \tag{50}$$

https://doi.org/10.1017/S0022377803002666 Published online by Cambridge University Press

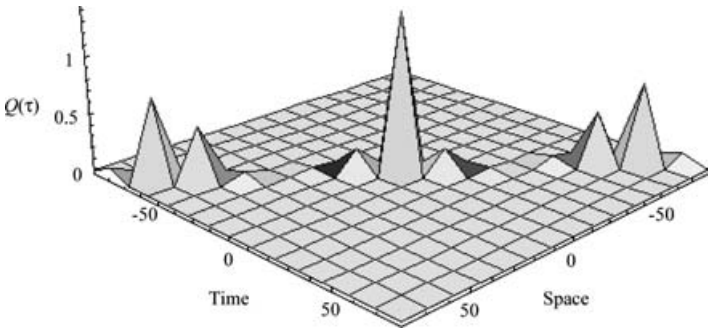

Figure 7. This figure represents the three-dimensional form of (49), the axes representing that equation. The representation here typifies the 'bright' soliton as opposed to Figs 2 and 6.

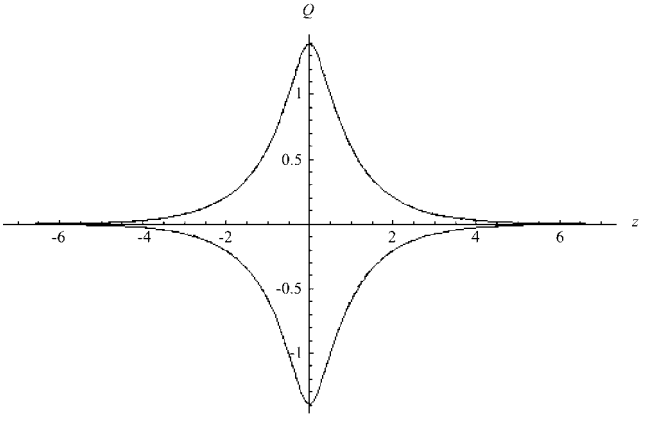

Figure 8. Plot of the non-topological dark soliton (49) with quintic term (continuous curves) and without quintic term (dotted curves) using the same parameters. The pseudo-potential structure is related to Fig. 1(d).

This type of soliton is equivalent to that given in Mihalach et al. (2002). Figure 8 is a plot of the non-topological dark-type wave related to the right small potential well (upper continuous curve) of Fig. 1(d) and the left small potential well (lower continuous curve). From (49) and (50), we see that this type of soliton is valid also for $g = 0$ and the usual non-singular soliton is just the case of (49) and (50) for $g = a = 0$. That means this type of soliton may be treated perturbatively when g is small. The corresponding black soliton solutions for the cubic NLSE are also plotted in Fig. 8 by point lines under the same parameters, except $g = 0$. From Fig. 8, we see that the effects of quintic nonlinear term enhances the amplitude and width of the soliton. Figure 7 represents Fig. 8 in three dimensions.

For the last characteristic structure of the pseudo-potential shown by Fig. 1(e), the corresponding period solution has the form

$$Q(\tau) = \pm \frac{\mathrm{sn}(\tau)}{\sqrt{a\mathrm{dn}^2(\tau) + b\mathrm{sn}^2(\tau)}} \tag{51}$$

https://doi.org/10.1017/S0022377803002666 Published online by Cambridge University Press

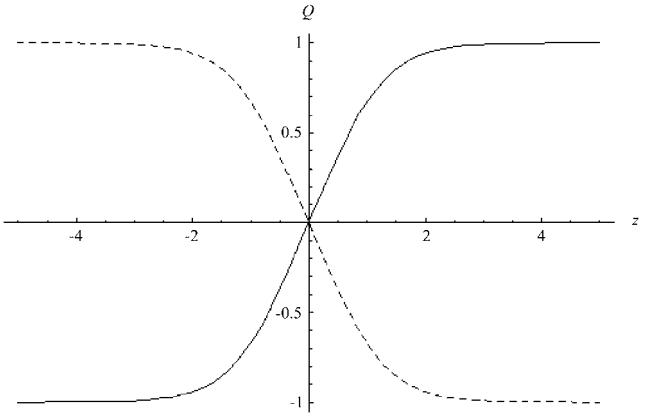

Figure 9. A plot of the second type of symmetric topological kink (continuous curve) and anti-kink (dotted curve) solitary wave solution (56) related to the pseudo-potential structure of Fig. 1(e).

which can be obtained from (21) by selecting $\phi(\tau)$ as

$$\phi(\tau) = \frac{\mathrm{dn}(\tau)}{\mathrm{sn}(\tau)} \tag{52}$$

with the parameters being fixed as

$$C = \frac{2m^2-1}{2b} + \frac{2g-3b}{12b^3k}, \quad a = -\frac{2g-2(2m^2-1)b^3k^2-b}{4m^2(m^2-1)bk^2}, \tag{53}$$

and

$$\omega = \frac{1}{2}(1-2m^2)k^2 + \frac{3}{4b} - \frac{g}{2b^2} - \frac{\omega_1^2}{4k^2} \tag{54}$$

while b is given by

$$12k^4b^4 - 8g(2m^2-1)k^2b^2 - 3b^2 + 8bg - 4g^2 = 0. \tag{55}$$

Similarly, when the modulus m of the Jacobi elliptic functions tend to one, the periodic solution (51) with (52)–(55) reduces to a new type of symmetric topological kink (or anti-kink) soliton:

$$Q(\tau) = \pm\frac{\mathrm{Sinh}(\tau)}{\sqrt{a\mathrm{Sinh}^2(\tau)+b}} \tag{56}$$

with $g>0,\ b>0,\ G>3a/4,\ a>0$ and

$$C = \frac{1}{3}\frac{3a-4g}{(a-2g)a}, \quad \omega = \frac{\omega_1^2a^4+4g^2-6ga+2a^2}{2a^2(a-2g)}, \quad k^2 = \frac{2g-a}{2a^2}, \quad b = \frac{3(a-2g)a}{3a-4g}. \tag{57}$$

In Fig. 9 we plot the typical kink (continuous curve) and anti-kink (dotted curve) solitons shown by (56) and (57). From (57), we can see that when $g=0, k$ becomes purely imaginary. That means this type of soliton is also induced by the quintic term of the NLSE (2) and cannot be treated perturbatively from the cubic NLSE. Consequently there are no three-dimensional plots for Fig. 1(e), as they appear simply as a plane.

https://doi.org/10.1017/S0022377803002666 Published online by Cambridge University Press

6. Results and discussion

In summary, by changing the envelope solution of the quintic NLSE to an equivalent pseudo-energy form of a classical quasi-particle and by means of the known periodic solutions of the ϕ^4 model, we can obtain quite an abundance of periodic wave solutions. By means of suitable limiting procedures for these periodic solutions, various solitons can be obtained. For the pseudo-potentials of the quasi-particle, there are five types of different characteristic structures. For the first such characteristic structure shown in Fig. 1(a), there is no periodic solution or soliton. For the other four types of characteristic structure, we obtain five types of periodic wave solution and five types of soliton. From these we have chosen to show three three-dimensional soliton graphs. The fifth appears only as a plane on the graph. To our knowledge there are no representations of the soliton as a three-dimensional graph.

For the second type of characteristic structure shown in Fig. 1(b), one type of explicit periodic solution which describes the motion of the quasi-particle at the left (or right) potential well is given. The corresponding soliton obtained from the periodic solution $m \to 1$ is a ring-type (or bell-shaped) symmetric non-topological gray soliton. A set of three-dimensional graphs has been developed for this.

Related to the third characteristic structure shown by Fig. 1(c), the explicit periodic solution also describes the motion of the quasi-particle at the left (or right) potential well. However, the corresponding soliton obtained from the periodic solution by $m \to 1$ is an asymmetric topological soliton. Again we show this in its three-dimensional form.

For the fourth type of characteristic structure shown in Fig. 1(d), there are two types of explicit periodic solutions which describe the periodic motions of the quasi-particle in the large potential well and two small potential wells, respectively. The soliton with the large period is the generalization of a special type of symmetric non-topological black soliton. This is also shown here in three dimensions.

For the last type of characteristic structure shown in Fig. 1(c), there exists only one symmetric potential well. The corresponding symmetric topological kink (anti-kink) soliton is different from that which was found in the fourth characteristic structure shown by Fig. 1(d). The related explicit periodic solution is also the generalization of the soliton. Since the parameters for this soliton are purely imaginary, there is no point of plotting a three-dimensional graph, as this will only produce a plane.

Except for the symmetric non-topological black soliton for the fourth type of characteristic structure, all the solitons are induced by the higher order nonlinearity (quintic term) of (2) and cannot be treated perturbatively. For the symmetric non-topological black soliton, the effects of the higher order nonlinear term enhances its amplitude and width compared with those for the cubic NLSE. Since the NLSE is one of the basic evolution models for nonlinear waves in various branches of physics, much work on Langmuir solitons in plasma, optical solitons and imaginary solitons has been stimulated and it is worth further study.

For the aforementioned consequences in plasma physics, we underline laser interaction in inhomogeneous plasmas as driving pseudo-Langmuir waves with very large amplitude longitudinal oscillations (Hora et al. 1984; Eliezer and Hora 1989) which have to be discussed for the electron acceleration to be of the order of very high energies (Hora et al. 2000). The properties of the nonlinear (ponderomotive)

forces in laser produced plasma have a general and unique role as the preferred solution to the Korteweg–de Vries equation, where the inclusion of dissipation by collisional damping clearly indicates the change from the initial non-soliton behavior into the soliton properties of laser–plasma interaction (Hora 2000).

References

Abramowitz, M. and Stegun, I. A. 1972 *Handbook of Mathematical Functions*. New York: Dover.

Agüero, M. 2001 *Phys. Lett. A* **278**, 260.

Cloot, A., Herbst B. M. and Weidman J. A. C. 1990 *J. Comput. Phys*. **86**, 127.

Eliezer, S. and Hora, H. 1989 *Phys. Rep.* **172**, 339.

Farina, D. and Bulanov, S. V. 2001 *Phys. Rev. Lett*. **86**, 5289.

Hayata, K. and Koshiba, M. 1995 *Phys. Rev*. E **51**, 1499.

He, X. T. 1982 *Acta Phys*. **31**, 1317.

He, X. T. and Zhou, C. T. 1993 *J. Phys. A: Math. Gen*. **26**, 4123.

Hora, H., Lalaousis, P. and Eliezer, S. 1984 *Phys. Rev. Lett.* **53**, 1650.

Hora, H., Hoelss, M., Scheid, W., Wang, J. X., Ho, Y. K., Osman, F. and Castillo, R. 2000 *Laser Particle Beams* **18**, 135.

Hora, H. 2000 *Plasmas at High Temperature and Density* (ed. S. Roderer). New York: Springer.

Liu, Z. J. and He, X. T. 1984 *Chin. Sci. Bull.* **29**, 1328.

Lou, S. Y. and Ni, G. J. 1989 *Math. Phys*. **30**, 1614.

Lou, S. Y. 2001 *Commun. Theor. Phys*. **35**, 589.

Mihalach, D., Mazilu, D. and Crasoan L.-C. 2002 *Phys. Rev. Lett*. **88**, 073902.

Modena, A., Najmudin, Z. and Dangor, A. E. 1995 *Nature* **377**, 606.

Ruostekoski, J. and Anglin, J. R. 2001 *Phys. Rev. Lett*. **86**, 3934.

Sentoku, Y., Esirkepov, T. Zh. and Mima, K. 1999 *Phys. Rev. Lett*. **83**, 3434.

Serkin, V. and Hasegawa, A. 2000 *Phys. Rev. Lett*. **85**, 4502.

Ying, Y. and Tan, Y. 1996 *Phys. Lett.* A **216**, 247.

Zakharov, V. E. and Shabat, A. B. 1971 *Zh. Eksp. Teor. Fiz*. **61**, 118.

Zakharov, V. E. and Shabat, A. B. 1972 *Sov. Phys.–JETP* **34**, 62.

Zhonghao, Li., Lu, Li., Huiping, T. and Guosheng, Z. 2000 *Phys. Rev. Lett*. **84**, 4096.

Zhou, C. T., He, X. T. and Chen, S. G. 1992 *Phys. Rev.* A **46**, 2277.